# Chemical routes to materials



# Block copolymer-mediated synthesis of TiO<sub>2</sub>/ RuO<sub>2</sub> nanocomposite for efficient oxygen evolution reaction

Binod Raj KC<sup>1</sup>, Dhananjay Kumar<sup>2</sup>, and Bishnu Prasad Bastakoti<sup>1,\*</sup>

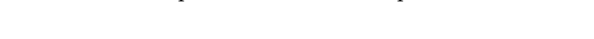
Received: 19 January 2024 Accepted: 22 April 2024 Published online: 5 June 2024

© The Author(s), 2024

### **ABSTRACT**

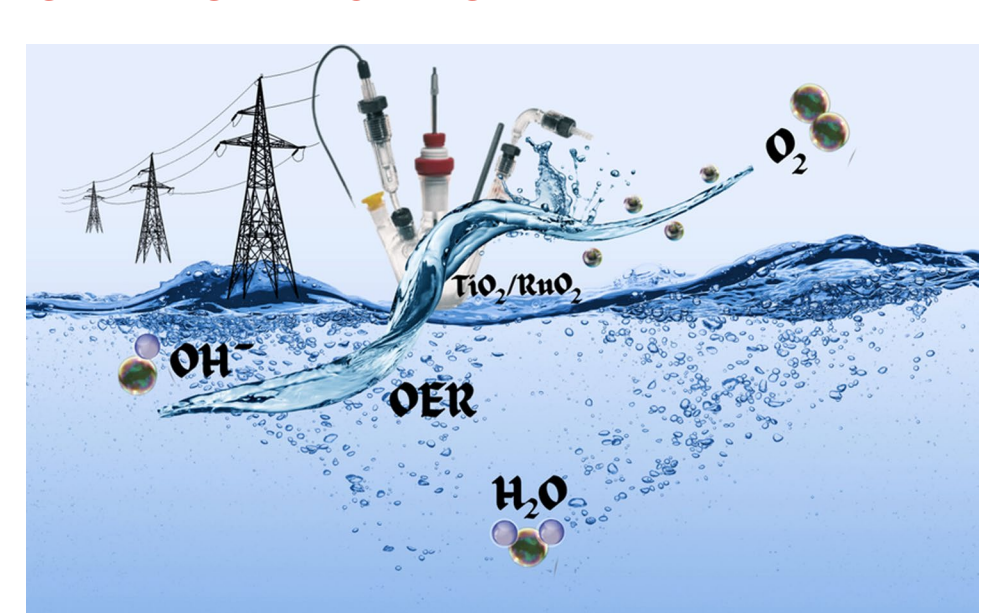
An amphiphilic block copolymer, poly (styrene-2-polyvinyl pyridine-ethylene oxide), was used as a structure-directing and stabilizing agent to synthesize TiO<sub>2</sub>/RuO<sub>2</sub> nanocomposite. The strong interaction of polymers with metal precursors led to formation of a porous heterointerface of TiO<sub>2</sub>/RuO<sub>2</sub>. It acted as a bridge for electron transport, which can accelerate the water splitting reaction. Scanning electron microscopy, energy-dispersive X-ray spectroscopy, transmission electron microscopy, and X-ray diffraction analysis of TiO<sub>2</sub>/RuO<sub>2</sub> samples revealed successful fabrication of TiO<sub>2</sub>/RuO<sub>2</sub> nanocomposites. The TiO<sub>2</sub>/RuO<sub>2</sub> nanocomposites were used to measure electrochemical water splitting in three-electrode systems in 0.1-M KOH. Electrochemical activities unveil that TiO<sub>2</sub>/RuO<sub>2</sub>-150 nanocomposites displayed superior oxygen evolution reaction activity, having a low overpotential of 260 mV with a Tafel slope of 80 mVdec<sup>-1</sup>.

Handling Editor: Pedro Camargo.



https://doi.org/10.1007/s10853-024-09702-5

<sup>&</sup>lt;sup>1</sup> Department of Chemistry, North Carolina Agricultural and Technical State University, 1601 E. Market St, Greensboro, NC 27411, USA <sup>2</sup> Department of Mechanical Engineering, North Carolina Agricultural and Technical State University, 1601 E. Market St, Greensboro, NC 27411, USA



### GRAPHICAL ABSTRACT

### Introduction

The rapid increase in the world's population and industrialization has resulted in a rising demand for energy supply, considered one of the topmost challenges over the past few decades [1]. Recently, more than two-thirds of world energy demands are still supplied by traditional carbon-based fossil fuels, which are finite and unsustainable [2]. Burning of fossil fuels is considered one of the main reasons for carbon dioxide emissions into the environment [3], causing global warming and climate change, instigating a search for alternative, renewable, and clean energy sources [1, 4–6]. Among various available alternative energy sources, hydrogen is one of the promising clean energy sources that are replacing traditional sources of fossil fuels as it is renewable and clean [1, 7]. It has zero carbon footprint, high energy density, and produces only water after combustion [1, 2]. Compared to hydrogen production using natural gas steam at high temperatures, electrochemical water splitting produces green hydrogen in an environmentally friendly concept toward a decarbonized future [1, 4, 8]. Electrolysis of water which involves two pivotal half reactions, one is hydrogen evolution reaction (HER) at cathode and another is oxygen evolution reaction (OER) at anode [3, 5, 9], has advantages over other processes as it offers the availability of unlimited reactants, scalable nature, safety, stability, and excellent purity of product [6, 10, 11].

In the past few decades, tremendous exertions have been made to find practically efficient, useful, abundant, and cost-effective electrocatalyst for OER since water electrolysis efficiency is usually reliant on slow reaction kinetics and unfavorable OER and HER thermodynamics [6]. The thermodynamic potential required for electrochemical water splitting is 1.23 V (0 V for HER and 1.23 V for OER) at 25 °C and 1 atm, but due to kinetic barrier of reaction, it requires usually higher potential than 1.23 V; hence, the excess potential required beyond 1.23 V is overpotential ( $\eta$ ) [12]. Tafel slope is a way to understand how fast a chemical reaction is happening at an electrode surface as well as to explicate the reaction mechanism [13]. The Tafel slope helps to understand the relationship between voltage and reaction rate. Empirically, the following Tafel relation has been well confirmed:  $\eta = a + b \log(j)$ , where ' $\eta$ ' defines the overpotential, 'j' denotes the current density, and 'b' is the Tafel slope [13]. Among the various reported OER electrocatalysts, ruthenium oxide (RuO<sub>2</sub>) is considered as a state-of-art catalyst having improved electrical conductivity, reversible redox properties, wide potential window, and, more importantly, lower overpotential and lower Tafel slope [14, 15]. Nonetheless, ruthenium is scarce and costly which



inhibits its excessive capitalization in bulky scale. So, one of the best strategies is to reduce the amount of catalyst used without sacrificing overall efficiency. This may be done by reducing the size of the catalyst to the nanometer level, which will increase the specific surface area. Due to particle growth during cycling and oxidation of ruthenium to higher oxidation states, OER activity of RuO2 nanoparticles is severely hampered by their poor cycling stability [9, 15, 16]. TiO<sub>2</sub> nanoparticles when combined with RuO<sub>2</sub> prevent corrosion of RuO<sub>2</sub> to RuO<sub>4</sub> or RuO<sub>4</sub>. The composites provide efficient pathways for charge transfer with improved stability [17, 18]. The use of less expensive transition metals/metal oxides  $(TiO_2)$  reduces the cost of catalyst [5, 19, 20]. Mixed metal oxides like TiO<sub>2</sub>/RuO<sub>2</sub> with oxygen vacancies expedite the water dissociation [21]. The presence of oxygen vacancies helps in reducing high energy barrier of water splitting by decreasing the activation energy [22, 23]. Until now, a number of strategies have been reported to improve OER performance of RuO<sub>2</sub>, such as elemental doping (Pt [24], Rh [9], and Zn [25]) and surface/interface engineering [26, 27], as well as forming composite [28–30]. As reported in the recent years, chromium-ruthenium oxide [16] and iridium-ruthenium oxide [31] displayed excellent OER performance at low overpotential with superior stability [16, 31]. Different researchers reported fabrication of RuO<sub>2</sub>/CeO<sub>2</sub> [30], RuO<sub>2</sub>/NiO [32], RuO<sub>2</sub>/ IrO<sub>2</sub> [33], and many more composite electrocatalysts with enhanced OER performance.

Surface design and modification of electrocatalysts are important in electrocatalytic conversion because they happen mostly on the surface of the catalyst. The surface chemistry can be changed by forming the heterostructure [34, 35]. The heterostructure materials are superior to those of a single nanomaterial. They have a large specific surface area, which assists in the exposure of more active sites and increases the contact area between catalyst and electrolyte, hence enhancing catalytic reaction. The intrinsic catalytic activity of the material can be enhanced by the redistribution of electrons between the two phases of the heterostructure interface [36, 37]. In heterojunction, electron rearrangement can be done at the interface of the heterostructure to alter the characteristics of the active sites to speed up the reaction kinetics. In fact, heterojunction catalysts frequently perform better in water electrolysis than single-component catalysts and are considered crucial in the field of electrocatalysis [37].

Herein, we report the strategies for constructing heterojunction and designing self-supporting nanocomposites via block copolymer-mediated one-pot synthesis method which is efficient for OER activities in an alkaline medium. The structure of the catalyst was directed and stabilized by using poly (styrene-2-polyvinyl pyridine-ethylene oxide), an amphiphilic block copolymer. Strong interactions between the polymer and metal precursors created a heterointerface that has a synergistic impact and serves as a bridge for electron transport between TiO<sub>2</sub> and RuO<sub>2</sub>, both of which can quicken the water splitting reaction. The synthesized nanocomposite catalyst showed competent catalytic activity for water splitting with an OER overpotential of only 260 mV for obtaining a current density of 10 mA/cm<sup>2</sup> with a Tafel slope of 80 mVdec<sup>-1</sup>.

## **Experimental section**

### **Materials**

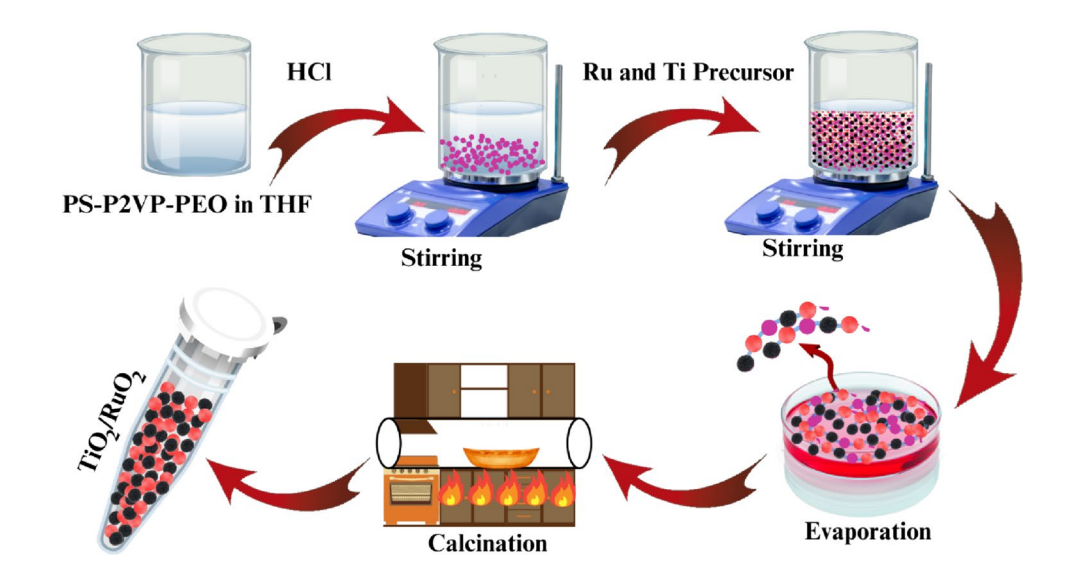
All the chemicals were used as received without further purification: titanium (IV) isopropoxide (TTIP) (97%, Alfa Aesar), ruthenium (III) chloride hydrate (RuCl $_3$ .3H $_2$ O, 99.99%, Thermo scientific), hydrochloric acid (HCl, 37%, Fisher Chemical), and poly (styrene-2-vinyl pyridine-ethylene oxide) (PS $_{13000}$ -P2VP $_{9000}$ -PEO $_{16500}$ ). During all the experiments, 18.2-M $\Omega$  Millipore deionized water was used.

## Synthesis of TiO2/RuO2 nanocomposites

TiO<sub>2</sub>/RuO<sub>2</sub> nanocomposites were prepared by sol-gel method (Fig. 1). A triblock copolymer PS-PVP-PEO was used as template and structure-directing agent. Forty mg of PS-P2VP-PEO was dissolved in 8 mL of tetrahydrofuran (THF), and 0.2 mL of HCl (37%) was added into it. Different concentrations of RuCl<sub>3</sub>.3H<sub>2</sub>O (100 mg, 150 mg, and 200 mg) were added into polymer solution containing 0.2 mL of TTIP. The samples were named as TiO<sub>2</sub>/RuO<sub>2</sub>-100, TiO<sub>2</sub>/RuO<sub>2</sub>-150, and  $TiO_2/RuO_2$ -200. The number represents the amount of RuCl<sub>3</sub>.3H<sub>2</sub>O added. The resulting solution was stirred for 2 h. The solution was left for drying in Petri dish for two days. After complete drying, the obtained samples were put for calcination at 500 °C for 3 h. Sixtyseven mg, 116.5 mg, and 170 mg samples were obtained for  $TiO_2/RuO_2-100$ ,  $TiO_2/RuO_2-150$ , and  $TiO_2/RuO_2-200$ ,



**Figure 1** Schematic illustration of synthesis procedure of TiO<sub>2</sub>/RuO<sub>2</sub> nanocomposites.



respectively, after calcination. For comparison, individual  ${\rm TiO_2}$  and  ${\rm RuO_2}$  samples were also prepared by using similar procedures.

### Characterization

Field emission scanning electron microscopy (FESEM, JEOL, JSM-IT800) was used to study the morphology of prepared samples. The FESEM elemental mapping and energy-dispersive X-ray spectroscopy (EDX) of sample were analyzed by using Oxford Instrument to study the chemical composition of the catalyst. Transmission electron microscopy (TEM, JEOL JEM-2100 Plus TEM) was used to observe the morphology and crystallinity of the catalyst. X-ray diffraction (XRD) (Rigaku, Miniflex 600) was used for confirming the presence of ruthenium oxide and titanium oxide and studying their crystal phase. Fourier transform infrared spectra (FTIR) of prepared sample and polymer were measured with IRTracer-100 FTIR spectrometer. Brunauer-Emmett-Teller (BET) analysis (Quantachrome Instruments NOVA 2200) was used for measurement of surface area of all calcined samples and their respective pore size and volume. The X-ray photoelectron spectroscopy (XPS) (Thermo Scientific ESCALAB™ XI-Al  $K\alpha$  and 200 eV) was used for the chemical analysis of calcined samples.

# Preparation of electrode and electrochemical measurements

Working electrode catalyst ink was prepared by mixing 4 mg of as-prepared finely ground electrocatalyst into 500 µL of ethanol (95%) followed by addition of 50 µL of Nation solution (5%w/w). The whole mixture was sonicated for 45 min to get homogeneous welldispersed ink. Then, copper foil (1 × 1 cm) was washed with deionized water followed by ethanol (95%) and dried in an oven. The catalyst ink was drop-casted on surface of clean copper foil followed by drying in oven at 60 °C. All the electrochemical experiments were performed in potentiostat (CH Instruments 760E) by using a three-electrode setup having catalyst (working electrode), the platinum electrode (counter electrode), and Ag/AgCl-saturated KCl (reference electrode) in 0.1-M KOH solution. Potentials were calibrated to reversible hydrogen electrode (RHE) scale by applying the equation  $E_{\text{(vs. RHE)}} = E_{\text{(Ag/AgCl)}} + 0.198 + 0.059 \text{pH}.$ 

### Results and discussion

The different diffraction peaks (Fig. 2) of anatase  $TiO_2$  (black line) and rutile  $RuO_2$  (red line) have been well matched with JCPDS: 02–0406 [38] and PDF: 731,469 [39], respectively. The diffraction pattern in the  $TiO_2$ /  $RuO_2$  nanocomposite clearly shows that most representative peaks of  $TiO_2$  and  $RuO_2$  maintained their



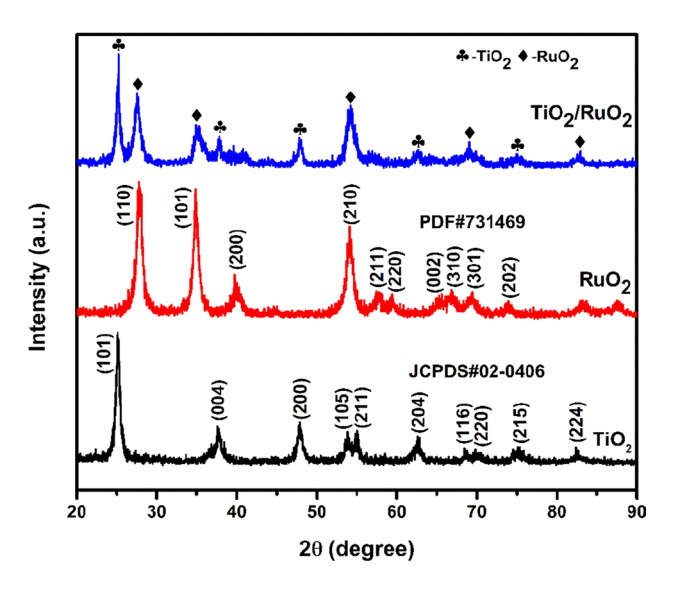


**Figure 2** XRD pattern of TiO<sub>2</sub>, RuO<sub>2</sub>, and TiO<sub>2</sub>/RuO<sub>2</sub> nanocomposite.

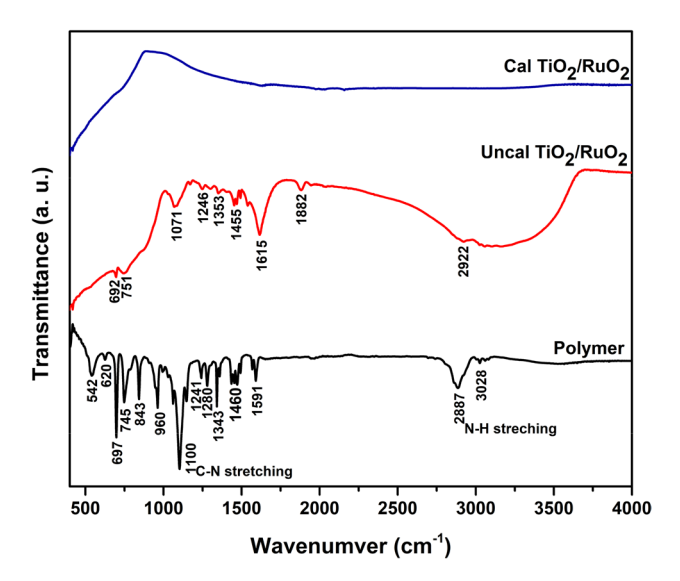


**Figure 3** Comparison of FTIR spectra of pure polymer, uncalcined, and calcined TiO<sub>2</sub>/RuO<sub>2</sub> nanocomposites.

2θ-positions. The existence of diffraction peaks for both TiO<sub>2</sub> and RuO<sub>2</sub> oxides in TiO<sub>2</sub>/RuO<sub>2</sub> nanocomposite provides proof that composite structures were made. The FTIR spectra of the polymer and TiO<sub>2</sub>/RuO<sub>2</sub> nanocomposites, both before and after calcination, were measured (Fig. 3). The intriguing findings reveal that in addition to the titanium and ruthenium source to the host polymer matrix, the N-H stretching vibration band at 2887 cm<sup>-1</sup> and C-N stretching band at 1100 cm<sup>-1</sup> diminish, and their wavenumber

is slightly shifted in the uncalcined composite sample, confirming the strong interaction of Ti or Ru with nitrogen group of triblock polymers. The region at 1085–1160 cm<sup>-1</sup> is mainly for C-O-C stretching due to the interaction of Ru and Ti cations with ether oxygen atoms in PEO (Fig. 3). The presence of hump-like peak at 3250 cm<sup>-1</sup> in uncalcined sample also indicates the presence of anions in the sample (OH<sup>-</sup>, Cl<sup>-</sup>) [40]. After calcination, all the signature peaks of polymer disappeared confirming the complete removal of block copolymer. The calcination not only removes the polymeric content but also induces crystallinity. The asprepared samples of TiO<sub>2</sub>/RuO<sub>2</sub> were amorphous in nature (Fig. S1). The FESEM image in Fig. 4a shows nanocomposites TiO<sub>2</sub>/RuO<sub>2</sub>-150 with homogeneous distribution of Ti, Ru, and O as shown in SEM elemental mapping in Fig. S2. The individual nanoparticles with heterojunction were clearly observed under TEM (Fig. 4b–e). The average particle size was 20–30 nm. The particle size was not uniform and larger when the polymer was not used in the synthesis confirming that the polymer has critical role to control the morphology of nanocomposites (Fig. S3). The elemental mapping of the TiO<sub>2</sub>/RuO<sub>2</sub> nanocomposite along with high-angle annular dark imaging (Fig. S4) further validates the successful fabrication of TiO<sub>2</sub>/RuO<sub>2</sub> nanocomposites. The HRTEM indicates the presence of clear crystalline materials without amorphous domains which are regarded as good electrocatalytic properties for water splitting. The TiO<sub>2</sub> nanoparticles are oriented in the (200) direction [1, 41] which are attached with nearby particles of RuO<sub>2</sub> oriented in the (101) direction [42, 43] indicating that interfaces are formed between different lattice fringes of the two materials, supporting the conclusion of interface coupling from XPS analysis. The lattice plane distance is calculated from HRTEM images, and values for  $d_{200}$  of anatase TiO<sub>2</sub> and  $d_{101}$  of rutile RuO<sub>2</sub> are determined to be 0.19 nm and 0.25 nm, respectively.

The isotherms of all nanocomposite samples exhibit a type-IV isotherm [44, 45] with hysteresis loop suggesting the presence of mesopores [46]. The change in hysteresis loop of different samples indicates change in pore size and pore volume, which is due to change in concentration of RuO<sub>2</sub> (Fig. S5). The presence of mesopores was further validated by pore size distribution curve as shown in Fig. S5b. The pore volume of different nanocomposites TiO<sub>2</sub>/RuO<sub>2</sub>-100, TiO<sub>2</sub>/RuO<sub>2</sub>-150, and TiO<sub>2</sub>/RuO<sub>2</sub>-200 calculated by DFT method was found to be 0.17 cc/g, 0.19 cc/g, and 0.15 g/



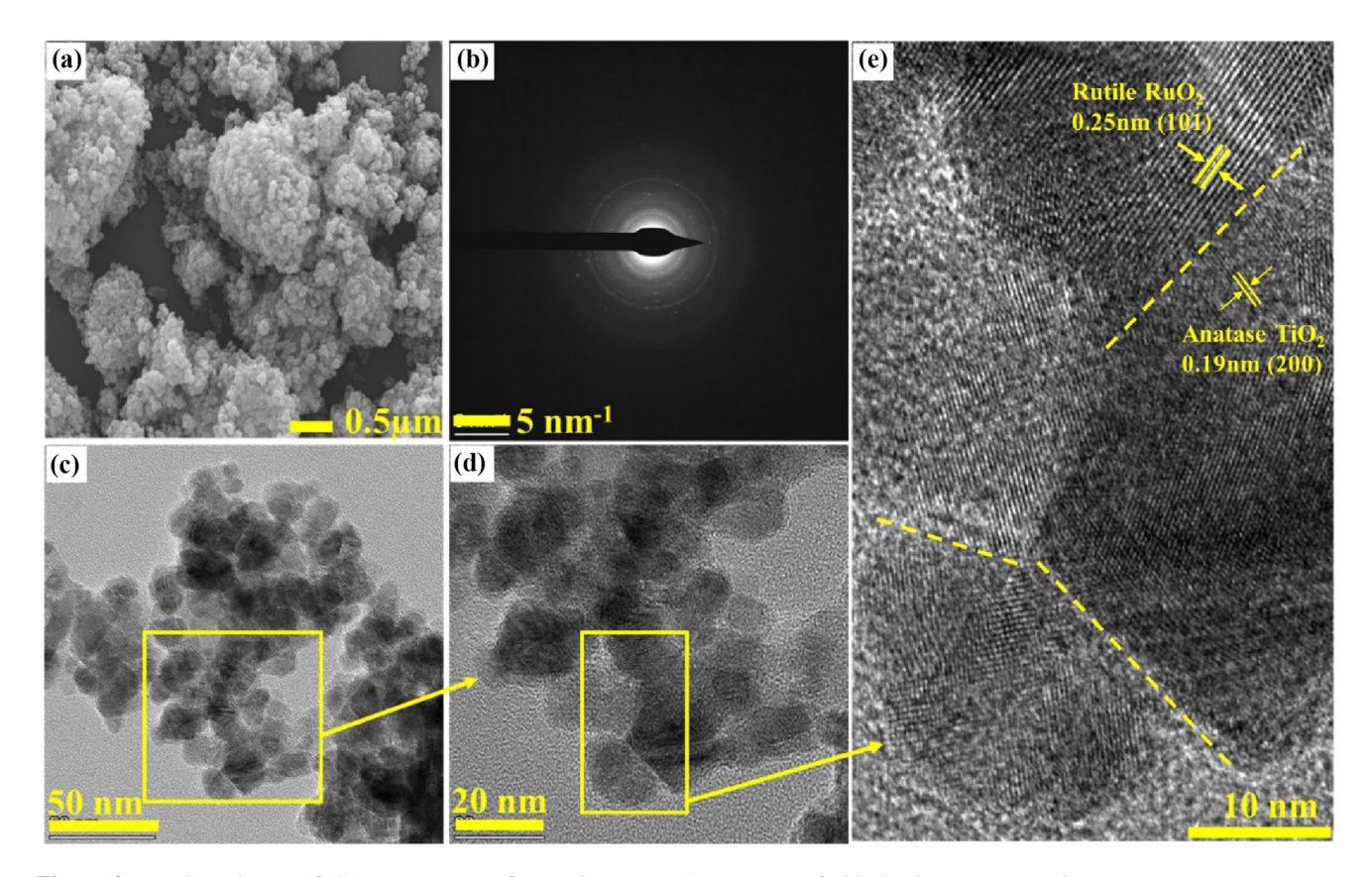
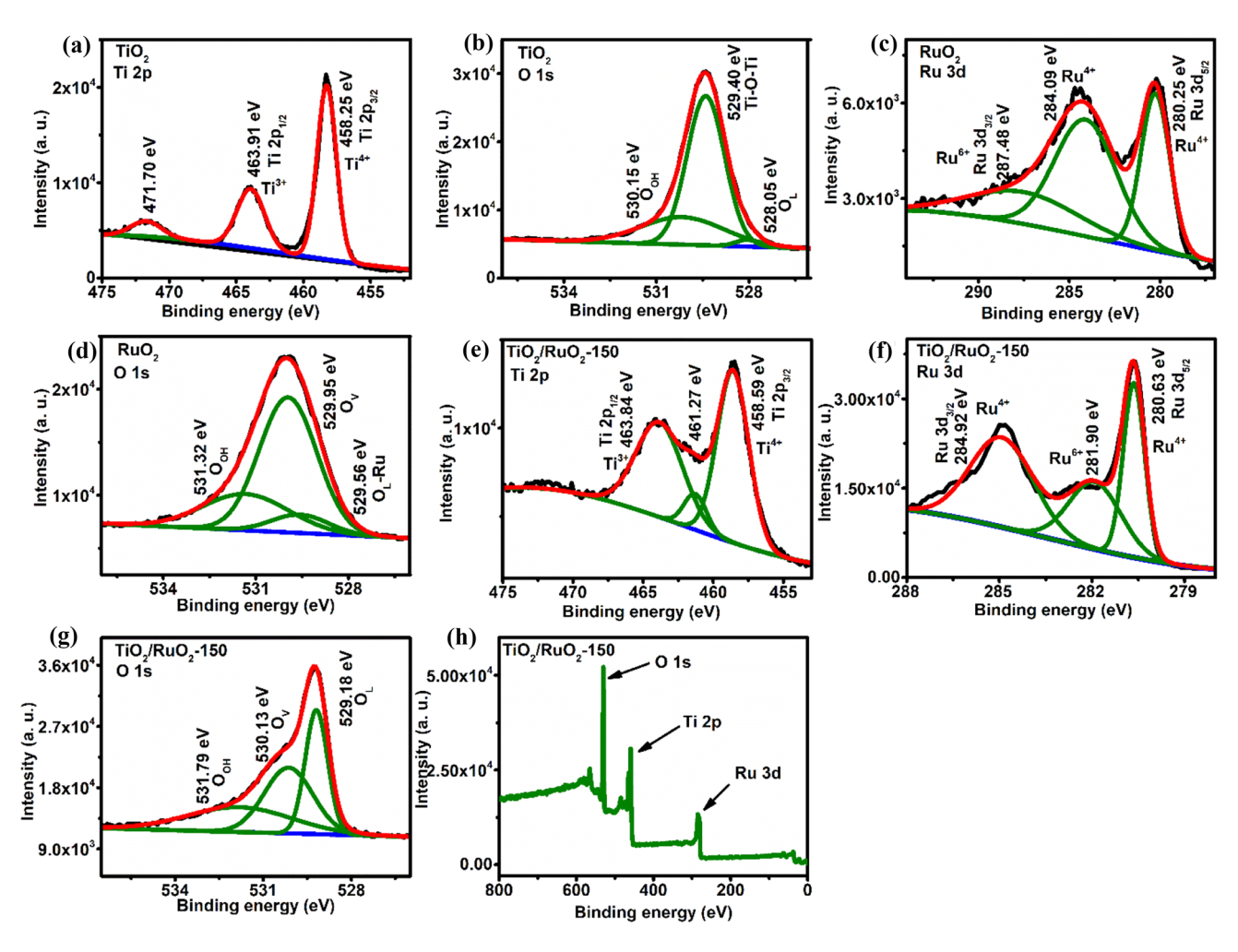


Figure 4 a FESEM images, b SAED pattern, c-d TEM images, and e HRTEM of TiO<sub>2</sub>/RuO<sub>2</sub> nanocomposites.

cc, respectively. The increase in porosity of materials (0.19 cc/g for  $TiO_2/RuO_2$ -150) further boosts the mobility of ions in electrolyte which results in better performance of electrocatalysis by increasing active sites [47]. The specific surface area of nanocomposites TiO<sub>2</sub>/RuO<sub>2</sub>-100, TiO<sub>2</sub>/RuO<sub>2</sub>-150, and TiO<sub>2</sub>/RuO<sub>2</sub>-200 calculated using multi-point BET method was found to be 21.69  $\text{m}^2/\text{g}$ , 27.52  $\text{m}^2/\text{g}$ , and 18.69  $\text{m}^2/\text{g}$ , respectively. The adsorption of  $N_2$  in case of TiO<sub>2</sub>/ RuO<sub>2</sub>-150 is higher as compared to that of TiO<sub>2</sub>/RuO<sub>2</sub>-100 and TiO<sub>2</sub>/RuO<sub>2</sub>-200 as indicated by adsorption/ desorption isotherm showing the highest surface area  $(27.52 \text{ m}^2/\text{g})$  which may be attributed to well dispersion of large number of RuO<sub>2</sub> nanoparticles with less agglomeration with TiO2 nanoparticles. This condition is advantageous for OER since charge transfer kinetics increase with increase in surface area of electrocatalysts because of exposure of more active sites by increasing the contact area between catalyst and electrolyte [36, 37]. These results of BET analysis are in good agreement with OER electrochemical performance of different nanocomposites. The XPS spectra

of Ti 2p clearly show the presence of Ti<sup>4+</sup> and Ti<sup>3+</sup> species [48], while the spectrum of Ru 3d indicates the existence of Ru<sup>4+</sup> and Ru<sup>6+</sup> species [4, 48, 49] as shown in Fig. 5 a, c, respectively. The deconvolved doublets peaks in composite as displayed in Fig. 5f with binding energies of 280.63 eV (Ru 3d<sub>5/2</sub>) and 284.92 eV (Ru  $3d_{3/2}$ ) are attributed to the Ru<sup>4+</sup>-O bond [1, 49], while peaks at 281.90 eV belong to Ru<sup>6+</sup>-O bond [49]. The Ru 3d<sub>5/2</sub> peak's positive binding energy shift is observed in TiO<sub>2</sub>/RuO<sub>2</sub>-150, indicating a possible partial electron transfer from Ru to the nearby Ti site at the TiO<sub>2</sub>/RuO<sub>2</sub> interface [4], as illustrated in Fig. 5c, f. The existence of high valance state of Ru in TiO2/RuO2 system with Ru<sup>6+</sup> and Ti<sup>3+</sup> may also cause the transfer of electron from Ru to Ti [50, 51]. The O 1s spectrum of nanocomposite is displayed in Fig. 5g with different peaks at 529.18 eV, 530.13 eV, and 531.79 eV representing lattice oxygen, defect oxygen, and adsorbed oxygen at surface of catalyst, respectively. The intensity of  $O_v$  peak distinctly increased in TiO<sub>2</sub>/RuO<sub>2</sub>-150 as compared to TiO<sub>2</sub> and RuO<sub>2</sub>, showing the oxygen vacancy defect [25]. Transfer of electrons and the existence of different





**Figure 5** XPS spectra of TiO<sub>2</sub>, RuO<sub>2</sub>, and TiO<sub>2</sub>/RuO<sub>2</sub>; **a** Ti 2p spectrum of TiO<sub>2</sub>, **b** 0 1s spectrum of TiO<sub>2</sub>, **c** Ru 3d spectrum of RuO<sub>2</sub>, **d** 0 1s spectrum of RuO<sub>2</sub>, **e** Ti 2p spectrum of TiO<sub>2</sub>/

 $RuO_2$ -150, **f** Ru 3d spectrum of  $TiO_2/RuO_2$ -150, **g** 0 1s spectrum of  $TiO_2/RuO_2$ -150, and **h** survey spectrum of composite  $TiO_2/RuO_2$ -150.

oxidation states of elements in electrocatalyst are beneficial for electrolysis of water.

TiO<sub>2</sub>/RuO<sub>2</sub> nanocomposites were tested for OER activities in 0.1-M KOH solution. Cyclic voltammetry (CV) of different samples (Fig. 6a–c) was performed to analyze electrochemical behavior of the surface oxidation states of nanocomposites in potential window of –0.1–1.7 V versus RHE with different scanning rates (20 mVs<sup>-1</sup>, 40 mVs<sup>-1</sup>, 60 mVs<sup>-1</sup>, 80 mVs<sup>-1</sup>, and 100 mVs<sup>-1</sup>). The observed oxidation state changes in CV during the potential scan at 0.6 V and 0.8 V versus RHE are responsible for redox transitions of Ru(III)/Ru(IV) and Ru(IV)/Ru(VI), respectively [52], and cathodic peak at low potential may be attributed to hydrogen absorption in the oxide lattice [52].

Moreover, the current density and area of CV curve are higher in TiO<sub>2</sub>/RuO<sub>2</sub>-150 than other composite materials, and it might be due to creation of higher number of heterojunction interfaces between TiO<sub>2</sub> and RuO<sub>2</sub> where electron cloud density of metal atom and oxygen has altered and is considered advantageous for oxygen evolution reaction [53]. The CV curve area and current were increased as the scan rate increases due to fast reaction kinetics. The shape of CV curve remains the same as it is on changing the scan rate which shows stability and high-performance catalyst. The OER performance of bare TiO<sub>2</sub> and RuO<sub>2</sub> is limited, as demonstrated in Fig. S6, while TiO<sub>2</sub>/RuO<sub>2</sub>-150 demonstrates comparatively significant OER activity.



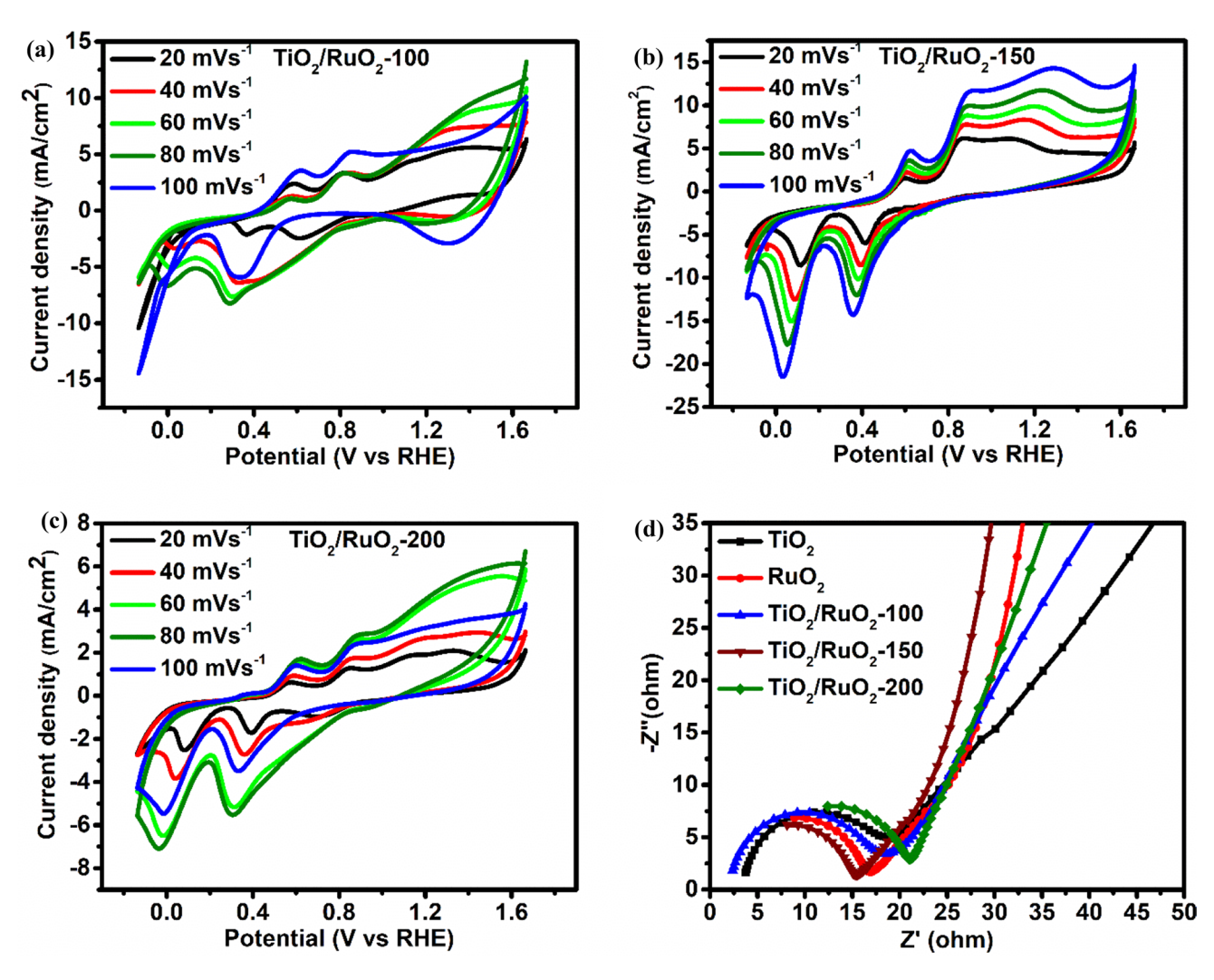


Figure 6 a-c Cyclic voltammetry of different composite samples and d Nyquist plot of all the samples.

The diameter of semicircle at high-frequency region of electrochemical impedance spectroscopy (EIS) is directly related to the charge transfer kinetics [8, 54–56] as well as intrinsic catalytic activity [57] of the electrocatalysts during the OER [52]. The representation of impedance is divided into real part (Z'or  $Z_{real}$ ) depicted on x-axis and imaginary part (Z" or  $Z_{imag}$ ) expressed on y-axis to form Nyquist plot where each point plotted on graph corresponds to an impedance at a specific frequency, with the imaginary part (Z") being represented as negative (Fig. 6d) [54, 58]. The impedance is represented as  $Z(\omega) = Z_{real} - jZ_{imag'}$ with  $Z_{\text{real}}$  denoting resistance (R) and  $Z_{\text{imag}} = 1/\omega C$ (where, C = capacitance and  $\omega$  = angular frequency) [59]. Nyquist plots obtained at high frequency for the different samples are shown in Fig. 6d. Among all

samples (TiO<sub>2</sub>, RuO<sub>2</sub>, TiO<sub>2</sub>/RuO<sub>2</sub>-100, TiO<sub>2</sub>/RuO<sub>2</sub>-150, and TiO<sub>2</sub>/RuO<sub>2</sub>-200), TiO<sub>2</sub>/RuO<sub>2</sub>-150 poses the smallest semicircle diameter or low impedance due to electrolyte ion diffusion, and it shows smaller charge transfer resistance (R<sub>ct</sub>) expedited by faster electron transfer and conductivity in an electrochemical reaction causing higher oxygen generation efficiency which may be due to interface coupling effect of TiO<sub>2</sub>/RuO<sub>2</sub> [3].

Linear sweep voltammetry (LSV) was recorded between 1.3 and 2.26 V versus RHE at 100 mV/s to study OER activity of different samples as shown in Fig. 7a. The overpotential at 10 mA/cm<sup>2</sup> parameter is used to compare the OER performance of different samples. The overpotential of TiO<sub>2</sub>/RuO<sub>2</sub>-150 at 10 mA/cm<sup>2</sup> is only 260 mV which is way better than RuO<sub>2</sub>, TiO<sub>2</sub>/RuO<sub>2</sub>-100, TiO<sub>2</sub>, and TiO<sub>2</sub>/RuO<sub>2</sub>-200



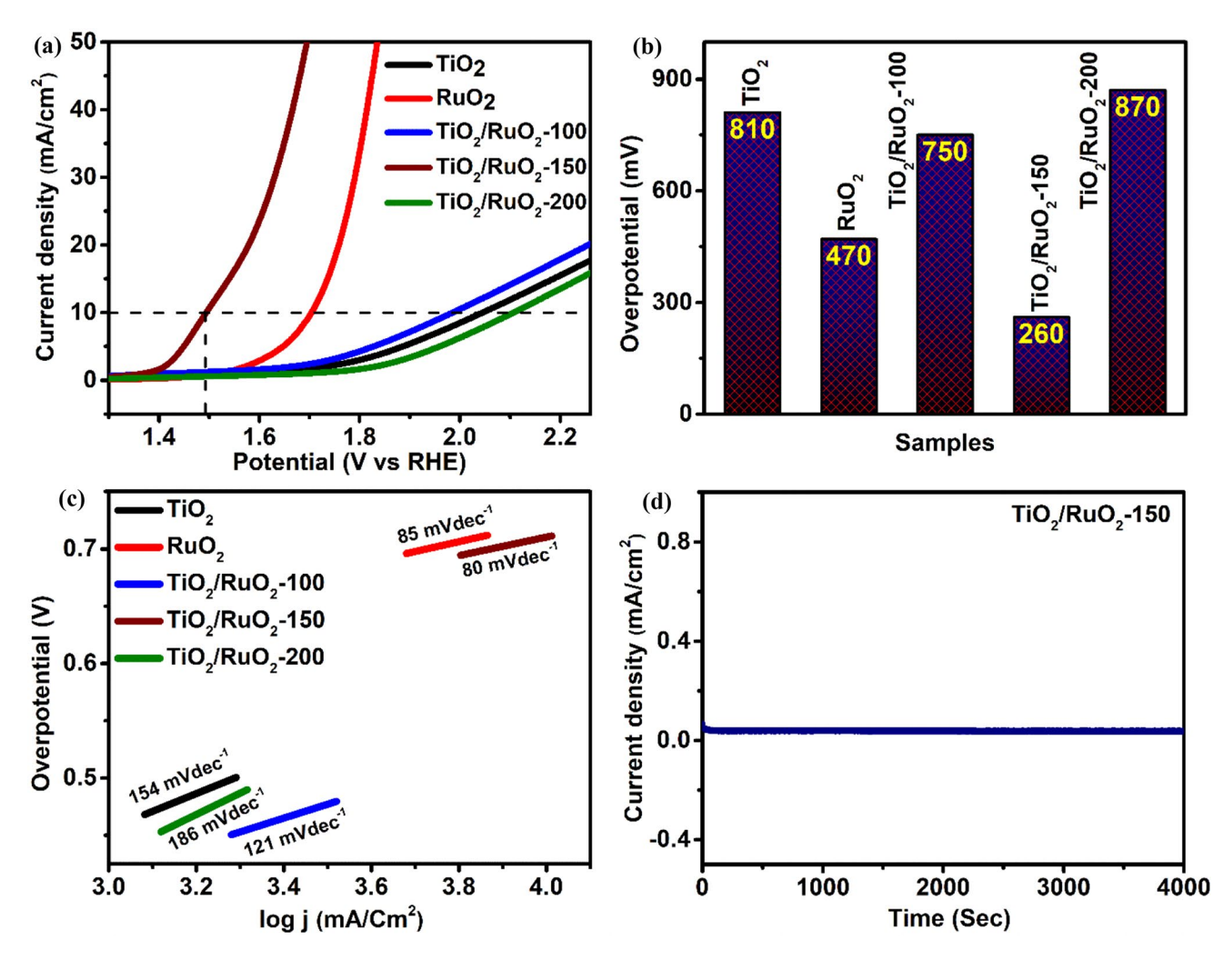


**Figure 7** a Linear sweep voltammetry curves of different samples measured between 1.2 and 2.2 V versus RHE, **b** graphical representation of overpotential of different samples, **c** Tafel plot of different samples, and  $d_{i-t}$  curve of nanocomposite TiO<sub>2</sub>/RuO<sub>2</sub>-150.

(Fig. 7b) since the surface area of  $\text{TiO}_2/\text{RuO}_2$ -150 is highest among other composites. The high surface area and greater pore volumes endeavor innumerable active catalytic sites [5] and make it easier for the free diffusion of oxygen and gas molecules [60], as well as high surface area helps for adsorption of more number of  $\text{OH}^-$  ion on its surface [5]. The comparison of recently reported Ru-based electrocatalysts for OER is shown in Table 1. The effective coupling of  $\text{RuO}_2$  and  $\text{TiO}_2$  may be the cause of the above-reported low value of the overpotential for the  $\text{TiO}_2/\text{RuO}_2$ -150 nanocomposite, which could be responsible for increasing the OER activity.

Tafel slope usually indicates the reaction kinetics of the catalysts. The OER Tafel slope of TiO<sub>2</sub>, RuO<sub>2</sub>, TiO<sub>2</sub>/RuO<sub>2</sub>-100, TiO<sub>2</sub>/RuO<sub>2</sub>-150, and TiO<sub>2</sub>/RuO<sub>2</sub>-200 is found to be 154 mVdec<sup>-1</sup>, 85 mVdec<sup>-1</sup>, 121 mVdec<sup>-1</sup>, 80 mVdec<sup>-1</sup>, and 186 mVdec<sup>-1</sup>, respectively, as displayed in Fig. 7c. Smaller the Tafel slope of catalysts, greater will be the reaction kinetics of catalysts [8, 13, 19, 25]. The smallest Tafel slope (80 mVdec<sup>-1</sup>) of TiO<sub>2</sub>/RuO<sub>2</sub>-150 shows the kinetics advantage of TiO<sub>2</sub>/RuO<sub>2</sub>, and this small value of sample might be because of nanocomposite constructed by nanoparticles of TiO<sub>2</sub> and RuO<sub>2</sub> which was beneficial for the mass transfer as well as diffusion and instant bubble release. Stability of catalyst is considered as an important parameter to



 Table 1
 Comparison of OER activity of Ru-based electrocatalysts

Catalysts	Methodology	Morphology	Electrolyte	Overpotential at 10 mV/cm <sup>2</sup> [mV vs. RHE]	Current [mA/ cm <sup>2</sup> ]	Tafel slope [mVdec <sup>-1</sup> ]	Ref.
TiO <sub>2</sub> /RuO <sub>2</sub>	Sol-gel	Nanoparticles	0.1-M KOH	260	10	80	This work
RuO <sub>2</sub> /CeO <sub>2</sub>	Hydrothermal	Nanosphere	1-M KOH	350	10	74	[15]
V <sub>2</sub> C-TiO <sub>2</sub>	Solvothermal	Nanoparticles	0.1-M KOH	425	50	189	[62]
RuO <sub>2</sub> /Co <sub>3</sub> O <sub>4</sub>	Impregnation	Nanocubes	1-M KOH	302	10	74.37	[53]
CuCo <sub>2</sub> O <sub>4</sub> /	Hydrothermal	Nanoneedles	1-M KOH	279	10	115	[63]
$CuO@RuO_2$	Electrodeposition						
$Au@TiO_2$	Spin coating	Nanoparticles/film	0.1-M KOH	350	10	99	[57]
$Ru/RuO_2\!\!-\!\!MoO_2$	Solid-phase reaction	Sphere	1-M KOH	260	10	65	[64]

evaluate the catalytic performance of prepared samples in order to fulfill the need for in-the-field applications [61]. The stability of catalyst is directly connected with cost-effectiveness, efficiency, and scale-up potential as well as long-term reliability of material. A stable catalyst can be used for long term without frequent replacement resulting in reduced overall operational costs, and stable catalyst also ensures consistent performance with predictable outcomes [61]. The OER *i*–*t* curve of TiO<sub>2</sub>/RuO<sub>2</sub>-150 is shown in (Figs. 7d and S7) which shows constant current density over the time at different applied potential.

#### Conclusions

This work represents TiO<sub>2</sub>/RuO<sub>2</sub> nanocomposite prepared by one-pot sol-gel method followed by calcination process. The stabilizing and structure-directing capabilities of block copolymer induce sterling heterointerface between TO<sub>2</sub> and RuO<sub>2</sub> which unclogs the transfer of electrons between the interfaces. Electron interaction of interface coupling effect between TiO<sub>2</sub> and RuO<sub>2</sub> nanoparticles with irregular surface showed improved OER activities at quite low overpotential of 260 mV with a Tafel slope of 80 mVdec<sup>-1</sup> in 0.1-M KOH. Therefore, this work provides an easy and effective way to synthesize block copolymer-mediated TiO<sub>2</sub>/RuO<sub>2</sub> electrocatalyst in water splitting for oxygen evolution reaction with potent activity and stability. Fabrication of TiO<sub>2</sub>/RuO<sub>2</sub> nanocomposite can also be scaled up by increasing the concentration of metal sources for various commercial applications. In future, different other block copolymers will be investigated as templates for preparing well-ordered nanostructure, size, shape, and spatial distribution of TiO<sub>2</sub> and RuO<sub>2</sub> nanoparticles as well as other metal oxides. Theoretical modeling and simulation of material can be done in order to predict structural and electronic properties for experimental design and to comprehend underlying mechanism of OER.

## Acknowledgements

This work is supported by the Center for Electrochemical Dynamics and Reactions on Surfaces, Department of Energy, via Grant DE-SC0023415. The samples were characterized in the Joint School of Nanoscience and Nanoengineering, a member of the Southeastern Nanotechnology Infrastructure Corridor and National Nanotechnology Coordinated Infrastructure, which is supported by the National Science Foundation (Grant ECCS-1542174). Authors thank Mr. Rabin Dahal and Mr. Moses D. Ashie for SEM and XPS measurements, respectively.

### **Author contributions**

B. R. K. was involved in data curation, formal analysis, investigation, validation, visualization, writing—original draft, and writing—review and editing. D. K. helped with supervision, writing—review and editing, and funding acquisition. B. P. B. participated in supervision, methodology, resources, writing—review and editing, and funding acquisition.



## **Funding**

Open access funding provided by the Carolinas Consortium.

# Data availability

The data presented in this study are available from the corresponding author upon reasonable request.

### **Declarations**

**Conflict of interest** The authors declare that they have no known conflicts of interest in terms of finance and personal relationships that could have appeared to influence the work reported here.

Ethical approval Not applicable.

**Supplementary Information** The online version contains supplementary material available at https://doi.org/10.1007/s10853-024-09702-5.

**Open Access** This article is licensed under a Creative Commons Attribution 4.0 International License, which permits use, sharing, adaptation, distribution and reproduction in any medium or format, as long as you give appropriate credit to the original author(s) and the source, provide a link to the Creative Commons licence, and indicate if changes were made. The images or other third party material in this article are included in the article's Creative Commons licence, unless indicated otherwise in a credit line to the material. If material is not included in the article's Creative Commons licence and your intended use is not permitted by statutory regulation or exceeds the permitted use, you will need to obtain permission directly from the copyright holder. To view a copy of this licence, visit http://creativecommons.org/licenses/by/4.0/.

### References

[1] Liu Y, Duan T, Xu L et al (2023) Electrocatalyst of RuO<sub>2</sub> decorating TiO<sub>2</sub> nanowire arrays for acidic oxygen evolution. Int J Hydrogen Energy 48:10737–10754. https://doi.org/10.1016/j.ijhydene.2022.12.051

- [2] Zhang J, Lin R, Zhao Y et al (2023) Modulation for RuO<sub>2</sub>/TiO<sub>2</sub> via simple synthesis to enhance the acidic oxygen evolution reaction. ACS Sustain Chem Eng 11:9489–9497. https://doi.org/10.1021/acssuschemeng.3c01881
- [3] Vijayapradeep S, Kumar RS, karthikeyan SC, et al (2024) Constructing micro-nano rod-shaped iron-molybdenum oxide heterojunctions to enhance overall water electrolysis. Mater Today Chem 36:101934. https://doi.org/10.1016/j. mtchem.2024.101934
- [4] Wang X, Wan X, Qin X et al (2022) Electronic structure modulation of RuO<sub>2</sub> by TiO<sub>2</sub> enriched with oxygen vacancies to boost acidic O<sub>2</sub> evolution. ACS Catal 12:9437– 9445. https://doi.org/10.1021/acscatal.2c01944
- [5] Vijayapradeep S, Logeshwaran N, Ramakrishnan S et al (2023) Novel Pt-carbon core–shell decorated hierarchical CoMo<sub>2</sub>S<sub>4</sub> as efficient electrocatalysts for alkaline/seawater hydrogen evolution reaction. Chem Eng J 473:145348. https://doi.org/10.1016/j.cej.2023.145348
- [6] Santhosh Kumar R, Karthikeyan SC, Ramakrishnan S et al (2023) Anion dependency of spinel type cobalt catalysts for efficient overall water splitting in an acid medium. Chem Eng J 451:138471. https://doi.org/10.1016/j.cej.2022. 138471
- [7] Ashie MD, Bastakoti BP (2024) Photocatalytic hydrogen evolution using mesoporous honeycomb iron titanate. Small. https://doi.org/10.1002/smll.202310927
- [8] Poudel MB, Logeshwaran N, Kim AR et al (2023) Integrated core-shell assembly of Ni<sub>3</sub>S<sub>2</sub> nanowires and CoMoP nanosheets as highly efficient bifunctional electrocatalysts for overall water splitting. J Alloys Compd 960:170678. https://doi.org/10.1016/j.jallcom.2023.170678
- [9] Wang Y, Yang R, Ding Y et al (2023) Unraveling oxygen vacancy site mechanism of Rh-doped RuO<sub>2</sub> catalyst for long-lasting acidic water oxidation. Nat Commun 14:1–10. https://doi.org/10.1038/s41467-023-37008-8
- [10] Lokesh S, Srivastava R (2023) CuAl layered double hydroxide as a highly efficient electrocatalyst for the electrolysis of water into hydrogen and oxygen fuels. Int J Hydrogen Energy 48:35–50. https://doi.org/10.1016/j.ijhydene.2022. 09.197
- [11] He C, Wang G, Parrondo J et al (2017) Pt/RuO<sub>2</sub>-TiO<sub>2</sub> electrocatalysts exhibit excellent hydrogen evolution activity in alkaline media. J Electrochem Soc 164:F1234–F1240. https://doi.org/10.1149/2.1661712jes
- [12] Wang S, Lu A, Zhong CJ (2021) Hydrogen production from water electrolysis: role of catalysts. Nano Converg 8(1):4. https://doi.org/10.1186/s40580-021-00254-x
- [13] Shinagawa T, Garcia-Esparza AT, Takanabe K (2015) Insight on Tafel slopes from a microkinetic analysis of



- aqueous electrocatalysis for energy conversion. Sci Rep 5:1–21. https://doi.org/10.1038/srep13801
- [14] Lee Y, Suntivich J, May KJ et al (2012) Synthesis and activities of rutile IrO<sub>2</sub> and RuO<sub>2</sub> nanoparticles for oxygen evolution in acid and alkaline solutions. J Phys Chem Lett 3:399–404. https://doi.org/10.1021/jz2016507
- [15] Galani SM, Mondal A, Srivastava DN, Panda AB (2020) Development of RuO<sub>2</sub>/CeO<sub>2</sub> heterostructure as an efficient OER electrocatalyst for alkaline water splitting. Int J Hydrogen Energy 45:18635–18644. https://doi.org/10. 1016/j.ijhydene.2019.08.026
- [16] Lin Y, Tian Z, Zhang L et al (2019) Chromium–ruthenium oxide solid solution electrocatalyst for highly efficient oxygen evolution reaction in acidic media. Nat Commun 10:162. https://doi.org/10.1038/s41467-018-08144-3
- [17] Osman JR, Crayston JA, Pratt A, Richens DT (2008) RuO<sub>2</sub>-TiO<sub>2</sub> mixed oxides prepared from the hydrolysis of the metal alkoxides. Mater Chem Phys 110:256–262. https://doi.org/10.1016/j.matchemphys.2008.02.003
- [18] Oakton E, Lebedev D, Povia M et al (2017) IrO<sub>2</sub>-TiO<sub>2</sub>: a high-surface-area, active, and stable electrocatalyst for the oxygen evolution reaction. ACS Catal 7:2346–2352. https://doi.org/10.1021/acscatal.6b03246
- [19] Qiu Z, Li Y, Gao Y et al (2023) 2D MOF-assisted pyrolysis-displacement-alloying synthesis of high-entropy alloy nanoparticles library for efficient electrocatalytic hydrogen oxidation. Angew Chemie Int Ed 62:e202306881. https:// doi.org/10.1002/anie.202306881
- [20] Zheng S, Li Q, Xue H et al (2020) A highly alkaline-stable metal oxide@metal-organic framework composite for highperformance electrochemical energy storage. Natl Sci Rev 7:305–314. https://doi.org/10.1093/nsr/nwz137
- [21] Kundu S, Vidal AB, Yang F et al (2012) Special chemical properties of RuO. J Phys Chem C 116:4767–4773. https:// doi.org/10.1021/jp2117054
- [22] Graciani J, Plata JJ, Sanz JF et al (2010) A theoretical insight into the catalytic effect of a mixed-metal oxide at the nanometer level: the case of the highly active metal/ CeO<sub>x</sub>/TiO<sub>2</sub> (110) catalysts. J Chem Phys 132:104703. https://doi.org/10.1063/1.3337918
- [23] Rodriguez JA, Ma S, Liu P et al (2007) Activity of CeO<sub>x</sub> and TiO<sub>x</sub> nanoparticles grown on Au(111) in the water-gas shift reaction. Science 318:1757–1760. https://doi.org/10.1126/science.115003
- [24] Wang J, Yang H, Li F et al (2022) Single-site Pt-doped RuO<sub>2</sub> hollow nanospheres with interstitial C for high-performance acidic overall water splitting. Sci Adv 8:1–11. https://doi.org/10.1126/sciadv.abl9271
- [25] Zhang D, Li M, Yong X et al (2023) Construction of Zn-doped RuO<sub>2</sub> nanowires for efficient and stable water

- oxidation in acidic media. Nat Commun 14:1–13. https://doi.org/10.1038/s41467-023-38213-1
- [26] Cui X, Ren P, Ma C et al (2020) Robust interface Ru centers for high-performance acidic oxygen evolution. Adv Mater 32:1–7. https://doi.org/10.1002/adma.201908126
- [27] Harzandi AM, Shadman S, Nissimagoudar AS et al (2021) Ruthenium core-shell engineering with nickel single atoms for selective oxygen evolution via nondestructive mechanism. Adv Energy Mater 11:1–12. https://doi.org/10.1002/ aenm.202003448
- [28] Mosallaei H, Hadadzadeh H, Ensafi AA et al (2023) Evaluation of HER and OER electrocatalytic activity over RuO<sub>2</sub>– Fe<sub>2</sub>O<sub>3</sub> nanocomposite deposited on HrGO nanosheets. Int J Hydrogen Energy 48:1813–1830. https://doi.org/10.1016/j.ijhydene.2022.10.026
- [29] Xie X, Zhang X, Tian W et al (2023) Tri-functional Ru-RuO<sub>2</sub>/Mn-MoO<sub>2</sub> composite: a high efficient electrocatalyst for overall water splitting and rechargeable Zn-air batteries. Chem Eng J 468:143760. https://doi.org/10.1016/j.cej. 2023.143760
- [30] Wu Y, Yao R, Zhang K et al (2024) RuO<sub>2</sub>/CeO<sub>2</sub> heterostructure anchored on carbon spheres as a bifunctional electrocatalyst for efficient water splitting in acidic media. Chem Eng J 479:147939. https://doi.org/10.1016/j.cej. 2023.147939
- [31] Hu C, Yue K, Han J et al (2023) Misoriented high-entropy iridium ruthenium oxide for acidic water splitting. Sci Adv 9:1–14. https://doi.org/10.1126/sciadv.adf9144
- [32] Yu T, Xu Q, Luo L et al (2022) Interface engineering of NiO/RuO<sub>2</sub> heterojunction nano-sheets for robust overall water splitting at large current density. Chem Eng J 430:133117. https://doi.org/10.1016/j.cej.2021.133117
- [33] Ma Z, Zhang Y, Liu S et al (2018) Reaction mechanism for oxygen evolution on RuO2, IrO<sub>2</sub>, and RuO<sub>2</sub>@IrO<sub>2</sub> coreshell nanocatalysts. J Electroanal Chem 819:296–305. https://doi.org/10.1016/j.jelechem.2017.10.062
- [34] Zhao M, Bastakoti BP, Li Y, et al (2015) Mesoporous TiO<sub>2</sub>/
  Zn<sub>2</sub>Ti<sub>3</sub>O<sub>8</sub> hybrid films synthesized by polymeric micelle assembly. Chem Commun 51:14582–14585. https://doi.org/10.1039/c5cc04903b
- [35] Bentley J, Bastakoti BP (2022) Block copolymer templated synthesis of mesoporous WO<sub>3</sub>/carbon nanocomposites. J Mater Sci 57:14772–14779. https://doi.org/10.1007/s10853-022-07564-3
- [36] Zhang Y, Liao W, Zhang G (2021) A general strategy for constructing transition metal Oxide/CeO<sub>2</sub> heterostructure with oxygen vacancies toward hydrogen evolution reaction and oxygen evolution reaction. J Pow Sour 512:230514. https://doi.org/10.1016/j.jpowsour.2021.230514



- [37] Li Z, Hu M, Wang P et al (2021) Heterojunction catalyst in electrocatalytic water splitting. Coord Chem Rev 439:213953. https://doi.org/10.1016/j.ccr.2021.213953
- [38] Zhang Y, Liu X, Yusoff M, Razali MH (2021) Photocatalytic and antibacterial properties of a 3D flower-like TiO<sub>2</sub> nanostructure photocatalyst. Scanning 2021:3839235. https://doi.org/10.1155/2021/3839235
- [39] Lim JY, Rahman G, Chae SY et al (2014) Highly stable RuO<sub>2</sub>/SnO<sub>2</sub> nanocomposites as anode electrocatalysts in a PEM water electrolysis cell. Int J Energy Res 38:875–883. https://doi.org/10.1002/er.3081
- [40] Naveen Kumar K, Saijyothi K, Kang M et al (2016) Improved electrical properties of Fe nanofiller impregnated PEO + PVP:Li+ blended polymer electrolytes for lithium battery applications. Appl Phys A Mater Sci Process 122:1–14. https://doi.org/10.1007/s00339-016-0212-7
- [41] Yuan H, Besselink R, Liao Z, Ten Elshof JE (2014) The swelling transition of lepidocrocite-type protonated layered titanates into anatase under hydrothermal treatment. Sci Rep 4:4584. https://doi.org/10.1038/srep04584
- [42] Ge R, Li L, Su J et al (2019) Ultrafine defective RuO<sub>2</sub> electrocatayst integrated on carbon cloth for robust water oxidation in acidic media. Adv Energy Mater 9:1901313. https://doi.org/10.1002/aenm.201901313
- [43] Park J, Lee JW, Ye BU et al (2015) Structural evolution of chemically-driven RuO<sub>2</sub> nanowires and 3-dimensional design for photo-catalytic applications. Sci Rep 5:11933. https://doi.org/10.1038/srep11933
- [44] Jian Z, Liu P, Li F et al (2014) Core-shell-structured CNT@ RuO<sub>2</sub> composite as a high-performance cathode catalyst for rechargeable Li-O<sub>2</sub> batteries. Angew Chemie Int Ed 53:442–446. https://doi.org/10.1002/anie.201307976
- [45] Thangappan R, Arivanandhan M, Dhinesh Kumar R, Jayavel R (2018) Facile synthesis of RuO<sub>2</sub> nanoparticles anchored on graphene nanosheets for high performance composite electrode for supercapacitor applications. J Phys Chem Solids 121:339–349. https://doi.org/10.1016/j.jpcs. 2018.05.049
- [46] Singh I, Birajdar B (2017) Synthesis, characterization and photocatalytic activity of mesoporous Na-doped TiO<sub>2</sub> nano-powder prepared via a solvent-controlled non-aqueous sol-gel route. RSC Adv 7:54053–54062. https://doi. org/10.1039/c7ra10108b
- [47] Subramani S, Rajiv S (2022) Fabrication of poly(3-methyl-thiophene)/poly(ethylene oxide)/ruthenium oxide composite electrospun nanofibers for supercapacitor application. J Mater Sci Mater Electron 33:9558–9569. https://doi.org/10.1007/s10854-021-07549-z
- [48] Nong S, Dong W, Yin J et al (2018) Well-dispersed ruthenium in mesoporous crystal TiO2 as an advanced

- electrocatalyst for hydrogen evolution reaction. J Am Chem Soc 140:5719–5727. https://doi.org/10.1021/jacs.7b13736
- [49] Manríquez ME, Noreña LE, Wang JA et al (2018) One-pot synthesis of Ru-doped ZnO oxides for photodegradation of 4-chlorophenol. Int J Photoenergy 2018:7605306. https:// doi.org/10.1155/2018/7605306
- [50] Holmin S, Näslund LÅ, Ingason ÁS et al (2014) Corrosion of ruthenium dioxide based cathodes in alkaline medium caused by reverse currents. Electrochim Acta 146:30–36. https://doi.org/10.1016/j.electacta.2014.09.024
- [51] Sathiya M, Rousse G, Ramesha K et al (2013) Reversible anionic redox chemistry in high-capacity layered-oxide electrodes. Nat Mater 12:827–835. https://doi.org/10.1038/ nmat3699
- [52] Audichon T, Napporn TW, Canaff C et al (2016) IrO<sub>2</sub> coated on RuO<sub>2</sub> as efficient and stable electroactive nanocatalysts for electrochemical water splitting. J Phys Chem C 120:2562–2573. https://doi.org/10.1021/acs.jpcc.5b118 68
- [53] Guo BY, Zhang XY, Ma X et al (2020) RuO<sub>2</sub>/Co<sub>3</sub>O<sub>4</sub> Nanocubes based on Ru ions impregnation into prussian blue precursor for oxygen evolution. Int J Hydrogen Energy 45:9575–9582. https://doi.org/10.1016/j.ijhydene.2020.01.182
- [54] Lazanas AC, Prodromidis MI (2023) Electrochemical impedance spectroscopy—A tutorial. ACS Meas Sci Au 3:162–193. https://doi.org/10.1021/acsmeasuresciau.2c000 70
- [55] Ray SK, Bastakoti BP (2023) Improved supercapacitor and oxygen evolution reaction performances of morphology-controlled cobalt molybdate. Int J Hydrogen Energy 51:1109–1118. https://doi.org/10.1016/j.ijhydene.2023.11. 003
- [56] Chen T, Wang F, Cao S et al (2022) In situ synthesis of MOF-74 family for high areal energy density of aqueous nickel-zinc batteries. Adv Mater 34:1–10. https://doi.org/ 10.1002/adma.202201779
- [57] Tahir A, ul-Haq T, Zubair U, et al (2023) Au/TiO<sub>2</sub> thin film with ultra-low content of gold: an efficient self-supported bifunctional electrocatalyst for oxygen and hydrogen evolution reaction. Catal Today 418:114078. https://doi.org/10.1016/j.cattod.2023.114078
- [58] Magar HS, Hassan RYA, Mulchandani A (2021) Electrochemical impedance spectroscopy (Eis): principles, construction, and biosensing applications. Sensors 21:6578. https://doi.org/10.3390/s21196578
- [59] Aguedo J, Lorencova L, Barath M et al (2020) Electrochemical impedance spectroscopy on 2d nanomaterial mxene modified interfaces: application as a characterization and



- transducing tool. Chemosensors 8:1–21. https://doi.org/10. 3390/chemosensors8040127
- [60] Li Y, Wang W, Cheng M et al (2023) Arming Ru with oxygen-vacancy-enriched RuO<sub>2</sub> sub-nanometer skin activates superior bifunctionality for pH-universal overall water splitting. Adv Mater 35:1–10. https://doi.org/10. 1002/adma.202206351
- [61] Zhang K, Zou R (2021) Advanced transition metal-based OER electrocatalysts: current status, opportunities, and challenges. Small 17:1–40. https://doi.org/10.1002/smll. 202100129
- [62] Zaka A, Mansoor MA, Asghar MA et al (2023) V2C MXene-TiO<sub>2</sub> nanocomposite as an efficient electrode material for oxygen evolution reaction (OER). Int J Hydrogen Energy 48:34599–34609. https://doi.org/10.1016/j.ijhyd ene.2023.05.230

- [63] Zhang P, Liu X, He H et al (2020) Engineering RuO<sub>2</sub> on CuCo<sub>2</sub>O<sub>4</sub>/CuO nanoneedles as multifunctional electrodes for the hybrid supercapacitors and water oxidation catalysis. J Alloys Compd 832:154962. https://doi.org/10.1016/j. jallcom.2020.154962
- [64] Fan Y, Zhang X, Zhang Y et al (2021) Decoration of Ru/RuO<sub>2</sub> hybrid nanoparticles on MoO<sub>2</sub> plane as bifunctional electrocatalyst for overall water splitting. J Colloid Interface Sci 604:508–516. https://doi.org/10.1016/j.jcis.2021.07.038

**Publisher's Note** Springer Nature remains neutral with regard to jurisdictional claims in published maps and institutional affiliations.

